Environmental Technology

ISSN: 0959-3330 (Print) 1479-487X (Online) Journal homepage: http://www.tandfonline.com/loi/tent20

Flocculation kinetics of low-turbidity raw water and the irreversible floc breakup process

Rodrigo de Oliveira Marques & Sidney Seckler Ferreira Filho

To cite this article: Rodrigo de Oliveira Marques & Sidney Seckler Ferreira Filho (2017) Flocculation kinetics of low-turbidity raw water and the irreversible floc breakup process, Environmental Technology, 38:7, 901-910, DOI: 10.1080/09593330.2016.1236149

To link to this article: http://dx.doi.org/10.1080/09593330.2016.1236149

ENVIRONMENTAL TECHNOLOGY, 2017
VOL. 38, NO. 7, 901–910
http://dx.doi.org/10.1080/09593330.2016.1236149

Taylor & Francis
Taylor & Francis Group

Flocculation kinetics of low-turbidity raw water and the irreversible floc breakup process

Rodrigo de Oliveira Marques and Sidney Seckler Ferreira Filho

Hydraulic and Environmental Engineering Department, Polytechnic School, University of Sao Paulo, Sao Paulo, Brazil

ABSTRACT
The main objective of this study was to propose an improvement to the flocculation kinetics model presented by Argaman and Kaufman, by including a new term that accounts for the irreversible floc breakup process. Both models were fitted to the experimental results obtained with flocculation kinetics assays of low turbidity raw water containing *Microcystis aeruginosa* cells. Aluminum sulfate and ferric chloride were used as coagulants, and three distinct average velocity gradient (G) values were applied in the flocculation stage (20, 40 and 60 s^{-1}). Experimental results suggest that the equilibrium between the aggregation and breakup process, as depicted by Argaman and Kaufman's original model, might not be constant over time, since the residual turbidity increased in various assays (phenomenon that was attributed to the irreversible floc breakup process). In the aluminum sulfate assays, the residual turbidity increase was visible when G = 20 s^{-1} (dosages of 60 and 80 mg L^{-1}). For the ferric chloride assays, the phenomenon was noticed when G = 60 s^{-1} (dosages of 60 and 80 mg L^{-1}). The proposed model presented a better fit to the experimental results, especially at higher coagulant dosages and/or higher values of average velocity gradient (G).

ARTICLE HISTORY
Received 4 June 2016
Accepted 8 September 2016

KEYWORDS
Flocculation kinetics; irreversible floc breakup; low turbidity; aluminum sulfate; ferric chloride

1. Introduction

Conventional drinking water treatment depends primarily on effective floc removal by sedimentation. Thus, effective floc formation without subsequent floc breakup is critical to create stable flocculation units. Yet, some aspects involved within floc formation and breakup processes are still unclear. The mathematical models available are proven as useful auxiliary tools in the evaluation of flocculation units in drinking water treatment plants (DWTPs), but still do not resemble real large-scale flocculation processes [1–3].

The mathematical modeling of the flocculation process has been addressed by a great number of researchers, using a variety of techniques [4]. In general, most of the techniques applied in flocculation studies focus on extracting information regarding floc structure, from magnified images. For instance, light microscopy was the most utilized technique for decades. However, the largest issue with this technique is the sampling procedure. In the procedure, damage to the floc structure is likely to occur and, to a minor extent, further aggregation of the particles can also occur. Both of these may compromise the accuracy of the results [5–7].

Nowadays, digital imaging plays a significant role in flocculation studies, since it allows quick evaluations of several different images and can also be combined with light microscopy. But, similar to light microscopy, this technique requires sample extraction, and thus damage to the flocs or particle aggregation can also occur. Some studies have taken advantage of in situ digital image capturing devices, which can determine several floc characteristics without any direct contact with the floc. The lack of contact prevents damage to the floc or an unintentional change to its properties. The biggest downside to this technique is that it requires extensive knowledge about photography procedures and expensive equipment [5,6,8–10].

Electron microscopy (EM) images are useful to evaluate the flocculation process, due to its intense magnification (over 10,000 times), which provides a more detailed perspective of floc microstructure and primary particle interaction. But, traditional EM techniques, that is, transmission electron microscopy and scanning electron microscopy (SEM), may cause damage to floc structure during sampling and sample preparation. In addition, EM is very expensive, requires a great amount of time for sample preparation, and it is

CONTACT Rodrigo de Oliveira Marques rodrigo.oliveira.marques@usp.br Departamento de Engenharia Hidráulica e Ambiental, Escola Politécnica, Universidade de São Paulo, Avenida Professor Almeida Prado, número 83, travessa 2 – Cidade Universitária, São Paulo, CEP 05508-900, Brazil

Supplemental data for this article can be accessed at doi.org/10.1080/ 09593330.2016.1236149

hardly available in DWTPs [5,6]. A novel, but more expensive EM approach called WetSEM minimizes the floc damage [11]. But, few applications have been reported [12,13].

Besides image analysis, light scattering is common in flocculation modeling. Particle size distribution is determined as a function of the light scattering pattern of the analyzed suspension. But, this device requires sample extraction from the vessel, usually by means of a peristaltic pump with recirculation, which may alter the floc shape. Similar to light scattering, light transmission requires the analysis of an extracted sample. But, the light transmission device changes the floc size indirectly. In addition, light transmission devices require a suspension with a high floc concentration, which sometimes may be difficult to obtain. Therefore, light transmission devices are rarely used for flocculation modeling. Individual particle measuring devices are also reported in literature for flocculation modeling, but with fewer applications. In this device, floc breakage may occur when the suspension flows through the analysis cell. This device may also be limited due to the floc breakage and the need for samples with low floc concentration [4–6,14–17].

The most recent advance in flocculation modeling is the application of computational fluid dynamics (CFD) techniques. Although researchers have gained a great deal of understanding when studying flow patterns in structures, multiphase systems' modeling does not describe flocculation units precisely. For instance, one of the most common models for flocculation units is the Lagrangian particle model. Because this model assumes the floc is a point mass, it does not fully consider the fractal nature of the floc, disregarding its porosity, for instance. Even though more research is needed to improve its precision, CFD is a promising technique for flocculation modeling. It is particularly promising because advances in computational tools will further enhance such models. Yet, these models require extensive knowledge of advanced mathematics, access to cutting-edge software, and time needed to elaborate, run, and validate each model [18–24].

A common disadvantage among most of the techniques presented is the relatively high cost of the equipment [4–6]. Another drawback is that these devices are not available on a daily basis in DWTPs. This is especially true for DWTPs in developing countries, which usually lack investments in laboratory infrastructure. Therefore, a more practical approach is required in these cases. The mathematical model proposed by Argaman and Kaufman [25] is still widely used. Valuable practical information can be obtained with this classical model by means of a simple jar test. The model can be useful for DWTPs in developing countries, which typically have jar test devices readily available [1–4,25–28].

Argaman and Kaufman's model was proposed in the early 1970s and addresses one of the main assumptions made in the development of the first flocculation kinetics models, that is, the one that claims that flocs do not break [1–4]. Nowadays, it is widely known that this assumption does not describe the flocculation process accurately and several authors have addressed the floc breakup process [29–37]. In their model, Argaman and Kaufman assume that both aggregation and breakup processes take place simultaneously, and that equilibrium between them is eventually reached. The model does not include the irreversible breakup process mentioned by recent research regarding floc regrowth capacity [14,16,38]. The irreversible breakup process suggests that the equilibrium between the aggregation and breakup rates might only be temporary, leading to a lower clarified water quality as the irreversible breakup process intensifies.

Practical experience has shown that floc formation needed for effective sedimentation is impaired in waters with low turbidity, such as those from surface eutrophic water sources containing cyanobacteria cells [1,2,39–42]. Research has shown that flocs formed between the cyanobacteria *Microcystis aeruginosa* and iron and aluminum salts present variable regrowth capacity. This suggests that the irreversible breakup process can be identified during the flocculation of water containing this type of microorganism [17].

The main objective of this work was to propose an improvement to the flocculation kinetics model presented by Argaman and Kaufman (1970), including a new term that accounts for the irreversible floc breakup process. Within this objective, both models (original and proposed) were fitted to experimental results obtained in flocculation.

2. Material and methods

2.1. Raw water stock preparation

In order to simulate low turbidity raw water, such as those found in surface eutrophic sources, water stocks from the public supply system were inoculated with pure cultures of the cyanobacteria species *M. aeruginosa*. These were grown as previously reported [43]. The cell density was maintained between 1.5 and 2.0×10^5 cells mL^{-1}, which is typical for eutrophic surface waters [44]. Residual chlorine present in the water from the public supply system was removed with sodium thiosulfate pentahydrate ($Na_2S_2O_3 \cdot 5H_2O$). The first physicochemical characterization included total alkalinity, total organic carbon (TOC), total hardness, total iron, total manganese, total dissolved solids, and turbidity. The analytical methods used are reported in the last edition of the Standard Methods for the Examination of Water and Wastewater [45]. The water stocks were then inoculated with pure cultures of *M. aeruginosa* and a second aliquot was collected, in which pH, temperature, and turbidity were measured [45]. Also, the zeta potential of the raw water stocks was determined with the aid of a Zetasizer Nano Z from Malvern®.

2.2. Flocculation kinetics assays

The flocculation kinetics assays were grouped accordingly to each coagulant dosage tested. Within each group, three tests were completed with different values of *G* (average velocity gradient) applied to the flocculation stage (slow mixing). The coagulants used in this study were aluminum sulfate – $Al_2(SO_4)_3{\cdot}18H_2O$ – and ferric chloride – $FeCl_3{\cdot}6H_2O$. The coagulant dosages (expressed in terms of mass of powder) used were 10, 20, 40, 60, and 80 mg L^{-1}. To maximize the sweep flocculation mechanism, as it is recommended for the removal of *M. aeruginosa* cells by sedimentation [17], the pH was maintained between 6.0 and 6.5 in the assays with aluminum sulfate, while in the assays with ferric chloride, it was kept around 8.0. For pH adjustment, NaOH and HCl solutions were used (both 0.1 N) [1,2,46,47].

Previous to the kinetic flocculation tests, preliminary studies were conducted to determine the volume of the NaOH and HCl solutions needed for pH adjustments, for each coagulant dosage used. For each coagulant dosage, a titration curve was prepared. This way, it was possible to make the pH adjustment simultaneously with the coagulation step, in the same way it is done in DWTPs at a large scale [1,2,48]. The assays were carried out in a jar test device with 12 jars of 2 L. In the coagulation stage (rapid mixing), the rotation speed was set to 236 rpm, corresponding to an average velocity gradient (*G*) of approximately 600 s^{-1}. The coagulation (detention) time selected was 30 s, to obtain a Camp Number (given by the product Gt) of 18,000 [48]. Immediately after the start of stirring, the coagulant and the NaOH or HCl solutions were simultaneously added in each of the 12 jars. After 30 s, the rotational speed was reduced to match the selected *G* value of the flocculation stage. The *G* values used were 20, 40, and 60 s^{-1}.

The following flocculation times were used: 2.5, 5.0, 7.5, 10.0, 12.5, 15.0, 17.5, 20.0, 30.0, 40.0, 50.0, and 60.0 min. A different flocculation time was assigned to each jar, that is, 2.5 min for the first jar, 5.0 min for the second jar, and so forth. Once the flocculation time was reached in a given jar, the stirring was stopped to initiate the sedimentation process. The time during which the fluid inside the jars remained under agitation after the stirring stopped, also called the non-ideal settling time, was determined as 90, 120, and 150 s for *G* values of 20, 40, and 60 s^{-1}, respectively.

After the non-ideal settling time, the real settling time was recorded. For this experiment, a total of 4 min was selected for sedimentation. After measuring the real settling time, an aliquot was collected from each jar for turbidity analysis.

The turbidity increase due to coagulant dosage was also recorded. Separate assays were done following the procedure previously described for the flocculation kinetics assay. In these assays, the stirring of the jar test was ceased immediately after the rapid mixing stage and aliquots were collected to determine turbidity and zeta potential of the coagulated water.

2.3. Mathematical modeling

The mathematical modeling was divided into two separate stages. First, the proposed model was developed using the equations from Argaman and Kaufman's original model. The second stage comprehended fitting both models (Argaman and Kaufman's original model and the proposed model) to the experimental results.

2.3.1. Mathematical development of the proposed model

The proposed model is an improvement of Argaman and Kaufman's original model, and is based on the assumption that during the floc breakup process, a portion of the flocs breaks in an irreversible way. Conceptually, the proposed improvement is shown in Figure 1.

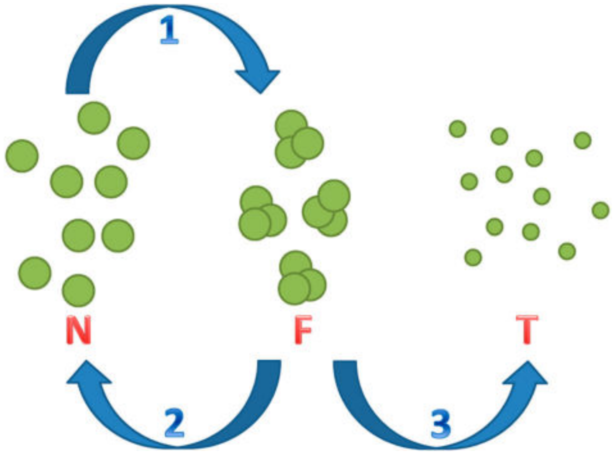

Figure 1. Conceptual view of the proposed model.

Note: *N* is the primary particles; *F* is the particles formed during the aggregation process and removable by sedimentation; *T* is the permanent residual particles not subject to aggregation and/or removal by sedimentation.

Figure 1 shows that the primary particles (*N*), previously destabilized in the coagulation step, aggregate (indicated by arrow 1) and form flocs that can be removed by sedimentation (*F*). Under certain conditions, these flocs then undergo a breakup process, creating again the primary particles *n* (indicated by the arrow 2).

The rate of change of the concentration of primary particles *N* can be described by Equation (1). All equations presented in this work assume that turbidity is an acceptable indicator of the concentration of colloidal particles in a colloidal suspension [28].

$$\frac{dN}{dt} = -K_A \cdot G \cdot N + K_B \cdot N_0 \cdot G^2, \tag{1}$$

where d*N*/d*t* is the rate of change in the concentration of primary particles *N* due to the sum of aggregation and breakup processes, *N* is the turbidity caused by the presence of primary particles (NTU), N_0 is the initial turbidity caused by the presence of primary particles (NTU), K_A is the aggregation constant (dimensionless), K_B is the breakup constant (s), *G* is the average velocity gradient (s^{-1}).

Equation (1) is the most common presentation of Argaman and Kaufman's original model. Considering a single-compartment batch reactor [1–3,25,26], the integral form of Equation (1) is presented by Equation (2).

$$N(t) = \frac{K_B}{K_A} \cdot G \cdot N_0 + \left(N_0 - \frac{K_B}{K_A} \cdot G \cdot N_0\right) \cdot e^{-K_A \cdot G \cdot t}, \tag{2}$$

where *N*(*t*) is the turbidity caused by the presence of primary particles at flocculation time *t* (NTU); *t* is the flocculation time (min).

A direct consequence of this model is that aggregation and breakup processes eventually reach equilibrium, thus *N*(*t*) remains constant over time when a steady floc size is reached [3,4,12,25,35,36].

In the proposed model, it is assumed that during the breakup of the *F* flocs, a portion of the broken flocs does not create new particles *N*, but generates *T* particles instead. *T* particles cannot be removed by sedimentation, nor do they form new flocs F. Thus, they create a permanent residual turbidity. In this work, it is assumed that this process is the irreversible floc breakup, indicated by the arrow 3 in Figure 1.

It was assumed that the term describing the irreversible breakup process of flocs *F* was similar to the aggregation process in Equation (1), but with a new constant, denominated K_C. So, the rate of change in the concentration of *F* particles is described by Equation (3).

$$\frac{dF}{dt} = K_A \cdot G \cdot N - K_B \cdot N_0 \cdot G^2 - K_C \cdot G \cdot F, \tag{3}$$

where d*F*/d*t* is the rate of change in the concentration of particles *F* formed due to the sum of the aggregation and breakup processes, *F* is the turbidity caused by the particles formed due to the aggregation process (NTU), and *Kc* is the irreversible breakup constant (s). The integral form of Equation (3) is presented by Equation (4).

$$F(t) = \frac{(K_A \cdot G \cdot N_0 - K_B \cdot G^2 \cdot N_0)}{(K_C \cdot G - K_A \cdot G)} \cdot (e^{-K_A \cdot G \cdot t} - e^{-K_C \cdot G \cdot t}), \tag{4}$$

where *F*(*t*) is the turbidity caused by the particles formed due to the aggregation process at flocculation time *t* (NTU).

The irreversible breakup process, which then generates a permanent residual turbidity *T*, is represented by Equation (5).

$$\frac{dT}{dt} = K_C \cdot G \cdot F, \tag{5}$$

where d*T*/d*t* is the rate of change of the concentration of particles due to the irreversible breakup process. The integral form of Equation (5) is presented by Equation (6).

$$T(t) = \left[\frac{K_C \cdot G^2 \cdot N_0 \cdot (K_A - K_B \cdot G)}{(K_C \cdot G - K_A \cdot G)}\right] \cdot \left[\frac{e^{-K_C \cdot G \cdot t}}{K_C \cdot G} - \frac{1}{K_C \cdot G} - \frac{e^{-K_A \cdot G \cdot t}}{K_A \cdot G} + \frac{1}{K_A \cdot G}\right], \tag{6}$$

where *T*(*t*) is the permanent residual turbidity caused by the particles not subject to aggregation and/or removal by sedimentation at flocculation time *t* (NTU).

2.3.2. Models-fitting procedure

The method of least squares was used to calibrate the kinetic constants and fit both models to the experimental data. The residual sum of squares (S_R) values were minimized with the aid of Microsoft Excel's 'Solver' function, using the GRG – Non-linear solution method [49–51].

Equation (2) was used to calculate residual turbidity as a function of time, to follow Argaman and Kaufman's original model. For the proposed model, residual turbidity was modeled as the sum of *N*(*t*) and *T*(*t*) fractions, as described by Equation (7).

$$N(t) + T(t) = \frac{K_B}{K_A} \cdot G \cdot N_0 + \left(N_0 - \frac{K_B}{K_A} \cdot G \cdot N_0\right) \cdot e^{-K_A \cdot G \cdot t} + \left[\frac{K_C \cdot G^2 \cdot N_0 \cdot (K_A - K_B \cdot G)}{(K_C \cdot G - K_A \cdot G)}\right] \cdot \left[\frac{e^{-K_C \cdot G \cdot t}}{K_C \cdot G} - \frac{1}{K_C \cdot G} - \frac{e^{-K_A \cdot G \cdot t}}{K_A \cdot G} + \frac{1}{K_A \cdot G}\right]. \tag{7}$$

3. Results

3.1. Qualitative characterization of the raw water stocks

Table 1 shows the qualitative characterization of the raw water stocks.

M. aeruginosa cell density and zeta potential averages, presented in Table 1, are within the range of preciously reported values for eutrophic surface waters [17,39–42,44]. The average turbidity of the raw water stocks, after inoculation with *M. aeruginosa* cells, was relatively low (only 2.5 NTU) [1,2]. Hence, the raw water stocks prepared effectively simulate a eutrophic surface water source with low turbidity.

3.2. Experimental results and the irreversible floc breakup process

3.2.1. Coagulant dosage

Figures 2 and 3 present the N_t/N_0 ratios for the assays with aluminum sulfate and ferric chloride, respectively, when $G = 20\ s^{-1}$. The influence of coagulant dosage was determined when $G = 20\ s^{-1}$, since the floc breakage was minimized with this G value, and trends were observed more clearly.

It is evident in Figures 2 and 3 that coagulant dosage plays a significant role in turbidity removal, as it would be expected [1,2]. For instance, dosages of 10 mg L^{-1} resulted in poor turbidity removal for both coagulants. Previous research has reported that sweep coagulation is an effective mechanism for floc formation in waters with low turbidity, where sedimentation is used for solid-liquid separation [1,2,17,39–42]. Therefore, in the assays with coagulant dosage of 10 mgL^{-1} (and within the pH range selected), the sweep coagulation mechanism was not maximized. When coagulant dosage was increased, turbidity removal also increased for both coagulants tested, which suggests that the sweep coagulation mechanism was favored and larger flocs were formed.

The most important aspect of the results presented in Figures 2 and 3 is related to the irreversible floc breakup process. Figure 2 shows that the dosages of 20 and 40 mg L^{-1} of aluminum sulfate effectively removed turbidity without any apparent subsequent deterioration of the clarified water quality (no residual turbidity increase) in higher flocculation times. Meanwhile, dosages of 60 and 80 mg L^{-1} both indicated a reduction of the clarified water quality after reaching a minimum residual turbidity value. Argaman and Kaufman's flocculation model assumes that a reduction of water quality does not occur. In their model, once aggregation and breakup reach equilibrium, it is constant over time. In the flocculation time range selected here, it was not possible to observe if the residual turbidity eventually stabilizes. Higher flocculation times, beyond 60 min, were not studied because they are unrealistic for conventional DWTPs. Therefore, it was assumed that the clarified water quality decline was a consequence of the irreversible floc breakup process. The turbidity increase seemed to be related with excessive coagulant dosage. Figure 4 shows that both models fitted to experimental results obtained in the assays with 60 and 80 mg L^{-1} of aluminum sulfate ($G = 20\ s^{-1}$).

It is clear that Argaman and Kaufman's original model presents a limitation when applied to the experimental results shown in Figure 4, since its curve eventually reaches a constant turbidity value that does not change over time. The proposed model, however, shows a residual turbidity increase over time. It was

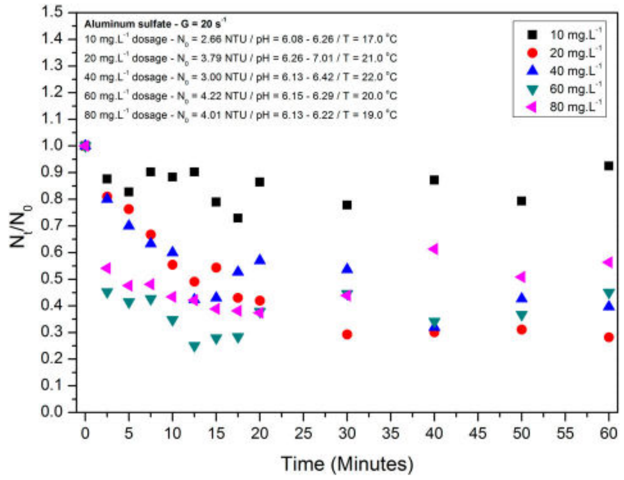

Figure 2. N_t/N_0 ratio for the aluminum sulfate assays with $G = 20\ s^{-1}$.

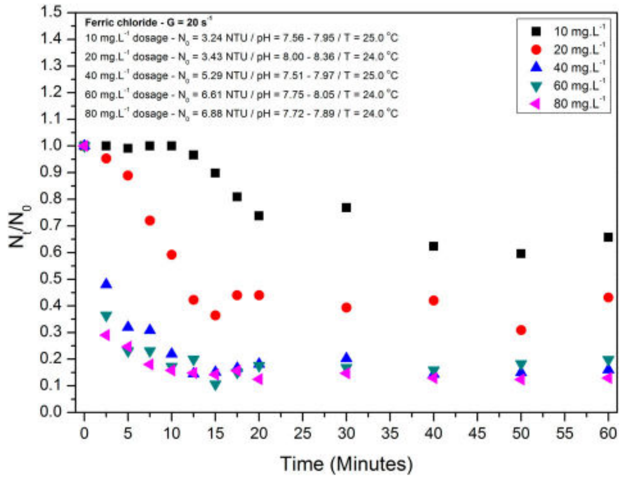

Figure 3. N_t/N_0 ratio for the ferric chloride assays with $G = 20\ s^{-1}$.

Table 1. Qualitative characterization of the raw water stocks.

Parameter	Unit	Average	Min.	Max.	σ
Conductivity	µS cm^{-1}	171.7	114.0	282.0	67.4
M. aeruginosa. cell density	cells mL^{-1}	1.7×10^5	8.1×10^4	4.8×10^5	1.3×10^5
pH	–	7.4	7.1	7.8	0.2
Temperature	°C	21.5	17.0	25.0	2.8
Total alkalinity	mg $CaCO_3$ L^{-1}	30.5	16.0	57.5	15.2
Total dissolved solids	mg L^{-1}	112.1	42.9	180.0	37.0
Total hardness	mg $CaCO_3$ L^{-1}	31.0	9.0	55.0	16.3
Total iron	mg Fe L^{-1}	0.04	0.0	0.1	0.04
Total manganese	mg Mn L^{-1}	0.002	0.0	0.0	0.002
TOC	mg C L^{-1}	2.9	1.8	6.0	1.4
Turbidity	NTU	2.5	2.0	3.4	0.5
Zeta potential	mV	−21.3	−13.0[a]	−27.9[a]	4.0

[a] Considering the zeta potential definition, the minimum values are closest to zero (0) and the maximum values are the most distant to zero (0).

assumed that the turbidity increase was a consequence of the irreversible floc breakup process.

Another interesting observation is that the residual turbidity increase was not shown in the assays with ferric chloride, as depicted in Figure 3. Recent studies indicated that the flocs formed between *M. aeruginosa* cells and aluminum are more susceptible to breakage than the ones formed with iron [17]. This suggests that the occurrence (or intensification) of the irreversible floc breakup process may also depend on the nature of the floc. But, detailed analyses of the floc structure and the internal bonds between each coagulant and the *M. aeruginosa* cells are beyond the scope of this work. As will be presented later, the irreversible floc breakup process was observed with increasing *G* values in ferric chloride assays also.

3.2.2. Zeta potential variation

This study also investigated the effect of the coagulant dosages on the variation of the zeta potential in the coagulated water. Figure 5 shows the change of the zeta potential in the coagulated water as a function of the coagulant dosages tested (expressed in terms of coagulant mass).

As seen in Figure 5, the addition of aluminum sulfate reduced the zeta potential, and it even exceeded the isoelectric point at a dosage of 80 mg L^{-1} ($\zeta_t = 2.2 \pm 0.3$ mV). However, the ferric chloride showed smaller reductions of the zeta potential, with the maximum reduction seen with 80 mg L^{-1} ($\zeta_t = -8.9 \pm 1.0$ mV). This difference can be explained by the behavior of Al^{+3} and Fe^{+3} ions in aqueous medium. The aluminum ions produce several hydrolyzed species that adhere to the surface of the colloidal particles, thus reducing the zeta potential. In the case of Fe^{+3} ions, the number of hydrolyzed species is smaller, as $Fe(OH)_3$ quickly forms and precipitates on the colloidal particles. And, after a certain dosage, further $Fe(OH)_3$ particles precipitate on top of the $Fe(OH)_3$ molecules that have already covered the colloidal particle. When this occurs, the measured zeta potential is that of the $Fe(OH)_3$ accumulated on the surface of the colloidal particle and not the zeta potential of the colloidal particle itself. This explains the apparent

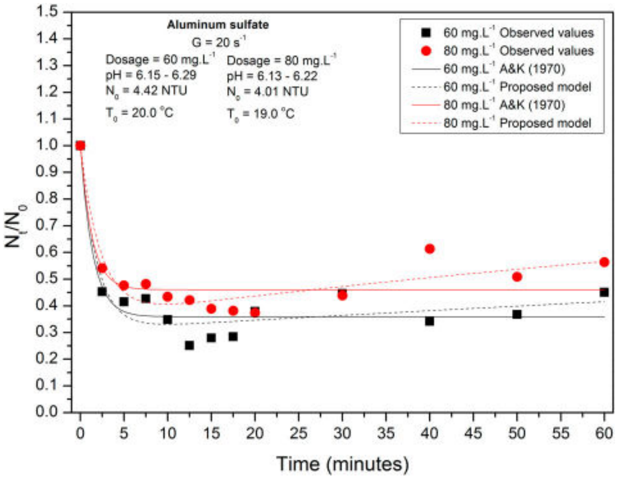

Figure 4. N_t/N_0 ratio for the aluminum sulfate assays with dosages of 60 and 80 mg L^{-1} and $G = 20$ s^{-1}, with both models fitted to the experimental results.

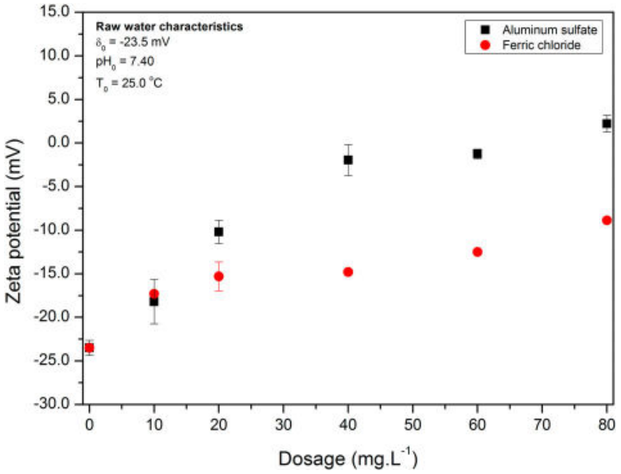

Figure 5. Influence of coagulant dosage (express in terms of coagulant mass) in the zeta potential of the coagulated water.

stabilization of the coagulated water's zeta potential, observed in Figure 4, even with the higher ferric chloride dosage [1,2,46,47]. This result suggests that reaching the isoelectric point is not required for effective turbidity removal. For example, a dosage of 20 mg L^{-1} of aluminum sulfate reduced the residual turbidity to one of its lowest values, and the zeta potential was only reduced to -10.2 ± 1.65 mV (far from the isoelectric point). In the case of ferric chloride, the same behavior was observed. A significant amount of turbidity was removed with a dosage of 40 mg L^{-1} of ferric chloride. But, in this case, zeta potential was reduced to -14.8 ± 1.8 mV. So, reaching the isoelectric point is not essential to successful floc formation. More importantly, the zeta potential should not be used as the only indicator of an effective solid-liquid separation process [1,2].

3.2.3. G value

Besides coagulant dosage, the *G* value utilized in a flocculation assay is an important variable in the irreversible floc breakup process. But, experimental results indicated that its influence is linked to coagulant dosage. For instance, as previously mentioned, for aluminum sulfate dosages of 60 and 80 mg L^{-1}, the irreversible floc breakup process was noticed when $G = 20\ s^{-1}$. When the *G* value was increased to 40 and 60 s^{-1}, the irreversible floc breakup process was intensified, as shown in Figures 6–7.

Again, it is possible to observe Argaman and Kaufman's model limitation as the experimental results were better represented by the proposed model. When evaluating ferric chloride assays, the importance of the *G* value is highlighted. In Figure 3, the irreversible floc breakup process was not apparently identified, most likely due to the strength of ferric chloride flocs, when comparing those with aluminum sulfate flocs [17]. However, the occurrence of the irreversible floc breakup was observed when higher *G* values were used. As an example, Figure 8 shows the experimental results in the assay with a ferric chloride dosage of 40 mg L^{-1}, all *G* values, and both models.

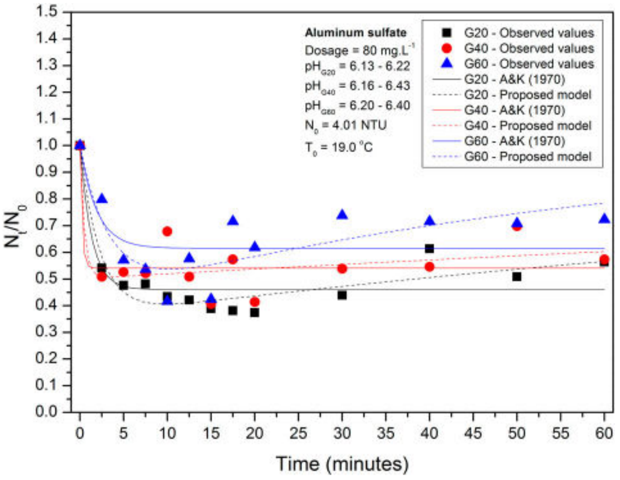

Figure 7. N_t/N_0 ratio for the aluminum sulfate assays with dosage of 80 mg L^{-1}, all *G* values, and both models fitted to the experimental results.

Figure 8 indicates that the irreversible floc breakup did not occur as strongly when *G* values were 20 and 40 s^{-1}. However, when the *G* value was increased to 60 s^{-1}, the residual turbidity increased, and the disparity between both models increased as well. When the ferric chloride dosage was increased to 60 mg L^{-1}, the same behavior was observed (Figure 9). Yet, when the dosage was increased to 80 mg L^{-1}, the occurrence of the irreversible breakup process was noticed when $g = 40\ s^{-1}$, as presented in Figure 10.

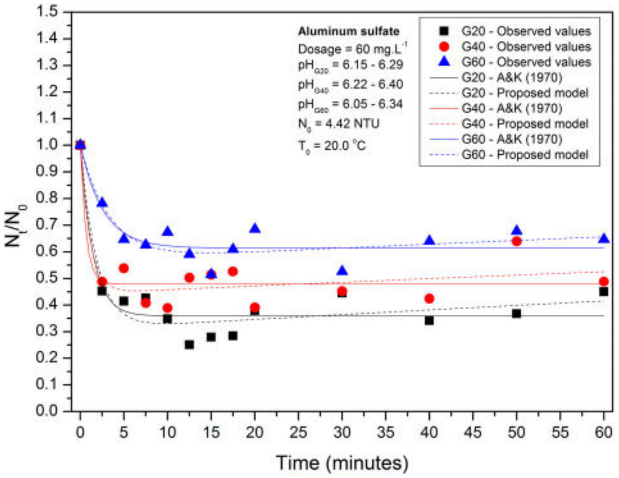

Figure 6. N_t/N_0 ratio for the aluminum sulfate assays with dosage of 60 mg L^{-1}, all *G* values, and both models fitted to the experimental results.

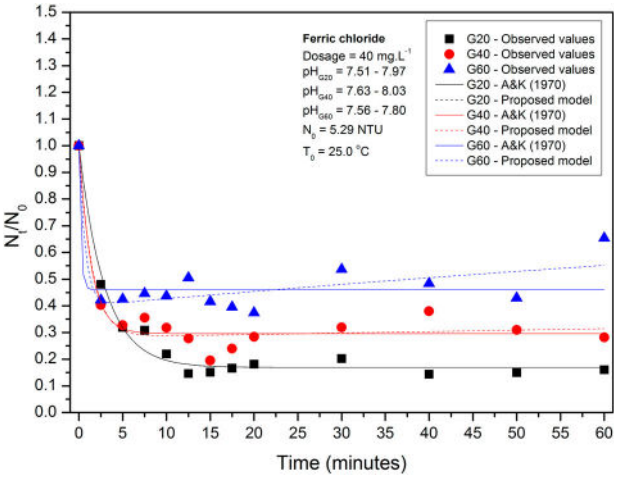

Figure 8. N_t/N_0 ratio for the ferric chloride assays with dosage of 40 mg L^{-1}, all *G* values, and both models fitted to the experimental results.

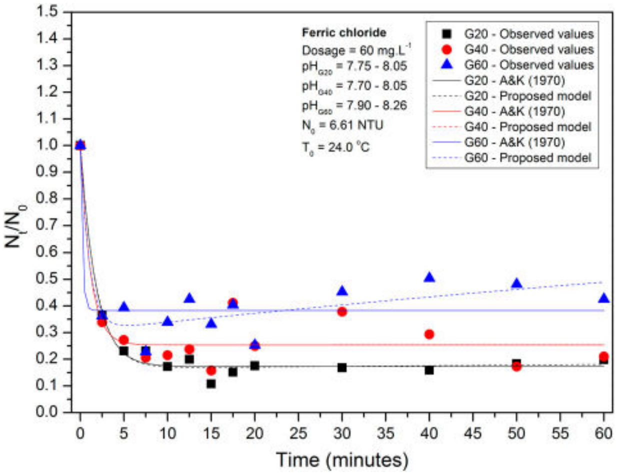

Figure 9. N_t/N_0 ratio for the ferric chloride assays with dosage of 60 mg L^{-1}, all G values, and both models fitted to the experimental results.

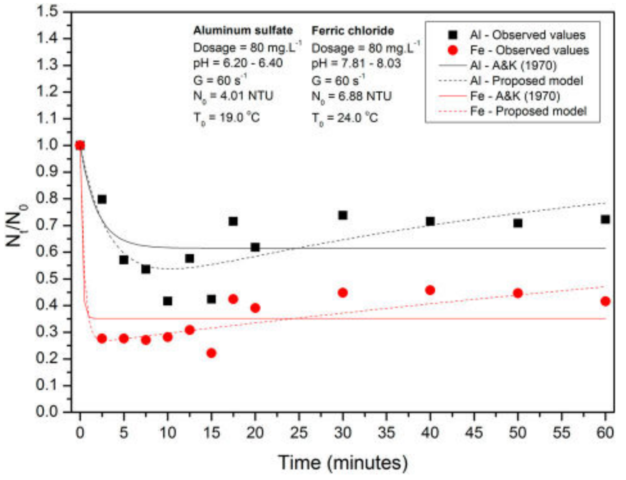

Figure 11. Models fitted to the experimental results obtained in the assays with 80 mg L^{-1} of coagulant dosage and $G = 60$ s^{-1}.

Another example can be seen in Figure 11, which shows both models fitting to the experimental results in the assays with 80 mg L^{-1} of coagulant dosage and $G = 60$ s^{-1}.

In the proposed model, the irreversible floc breakup process was assumed to be directly proportional to the G value used, as stated in Equation (5) (first-order rate expression). Variations of Equation (5) were not tested and should be further developed in future research.

3.2.4. Proposed model fitting

Table 2 presents all the values of the residual sum of squares (S_R) resulting from the fitting procedure of both models to the experimental results. All of the calibrated kinetic constants are found in the supporting information.

As seen in Table 2, in several assays the S_R values for both models were very similar. This result suggests that the effect of the irreversible breakup process was not significant for the assays where the S_R values were similar. It is also important to note that the proposed model is an improvement of Argaman and Kaufman's original model, and similar S_R values for these assays were expected. The main variables of the flocculation process studied, that is, coagulant dosage and G value, minimized the occurrence of the irreversible breakup process. Therefore, in these particular assays, both models present essentially the same behavior.

But, as it is indicated in Table 2, in several other assays the S_R values obtained from each model fitting procedure were substantially different. In such assays, S_R values resulting from the proposed model were lower than the ones from Argaman and Kaufman's original model. Assuming that the S_R values can be used as measure of 'goodness of fit' for non-linear models

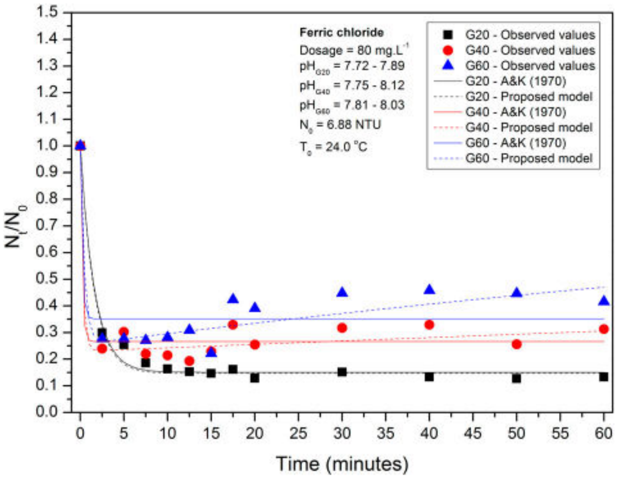

Figure 10. N_t/N_0 ratio for the ferric chloride assays with dosage of 80 mg L^{-1}, all G values, and both models fitted to the experimental results.

Table 2. Residual sum of squares (S_R) resulting from the fitting procedure of both models.

		Residual sum of squares (S_R)			
		Aluminum sulfate		Ferric chloride	
Dosage (mg L^{-1})	G (s^{-1})	A&K (1970)	Proposed model	A&K (1970)	Proposed model
10	20	0.28	0.27	0.46	0.45
	40	0.29	0.08	0.29	0.29
	60	0.28	0.15	0.30	0.30
20	20	0.17	0.17	0.90	0.77
	40	0.48	0.48	0.68	0.44
	60	0.67	0.40	0.66	0.66
40	20	0.49	0.49	0.34	0.34
	40	0.85	0.85	0.72	0.70
	60	0.76	0.76	1.79	1.12
60	20	0.82	0.67	0.38	0.38
	40	1.03	0.93	2.80	2.80
	60	0.59	0.51	3.45	2.15
80	20	0.94	0.46	0.35	0.36
	40	1.33	1.15	1.19	0.90
	60	2.46	1.23	3.65	1.44

[49–51], the results provide evidence that the proposed model is a better fit to the experimental results than Argaman and Kaufman's original model.

4. Conclusions

The experimental results obtained suggest that the equilibrium proposed by Argaman and Kaufman's flocculation model might not be constant over time, since a residual turbidity increase was detected in some of the assays. This phenomenon was attributed to the irreversible floc breakup process mentioned in recent research. At higher coagulant dosages and/or higher values of *G*, the inclusion of the irreversible breakup process in Argaman and Kaufman's original model resulted in a better fit of the experimental results. Further investigations are required in order to determine the actual causes of the irreversible floc breakup process and the variables that influence its intensification. Additionally, experimental results presented were obtained in flocculation kinetics assays of low-turbidity raw water, simulating a eutrophic surface water source. Therefore, it is critical to verify the applicability of the proposed model to different types of raw water.

Disclosure statement

No potential conflict of interest was reported by the authors.

ORCiD

Rodrigo de Oliveira Marques http://orcid.org/0000-0002-9285-055X

References

[1] Edzwald JK, editor. Water quality & treatment: a handbook on drinking water. 6th ed. New York: McGraw Hill; 2011.
[2] Crittenden, JC, Trussell RR, Hand DW, et al. MWH's water treatment: principles and design. 3rd ed. Hoboken: John Wiley & Sons; 2012.
[3] Moruzzi RB, de Oliveira SC. Mathematical modeling and analysis of the flocculation process in chambers in series. Bioprocess Biosyst. 2013;36:357–363.
[4] Thomas DN, Judd SJ, Fawcett N. Flocculation modelling: a review. Water Res. 1999;33:1579–1592.
[5] Jarvis P, Jefferson B, Parsons SA. Measuring floc structural characteristics. Rev Environ Sci Biotechnol. 2005;4:1–18.
[6] Bushell GC, Yan YD, Woodfield D, et al. On techniques for the measurement of the mass fractal dimension of aggregates. Adv Colloid Interface Sci. 2002;95:1–50.
[7] Clark MM, Flora JRV. Floc restructuring in varied turbulent mixing. J Colloid Interface Sci. 1991;147:407–421.
[8] Jarvis P, Jefferson B, Parsons SA. How the natural organic matter to coagulant ratio impacts on floc structural properties. Environ Sci Technol. 2005;39:8919–8924.
[9] Juntunen P, Liukkonen M, Lehtola M, et al. Characterization of alum floc in water treatment by image analysis and modeling. Cogent Eng. 2014;1:944767.
[10] Chakraborti RK, Atkinson JF, Van Benschoten JE. Characterization of alum floc by image analysis. Environ Sci Technol. 2000;34:3969–3976.
[11] Katz A, Bentur A, Kovler K. A novel system for in-situ observations of early hydration reactions in wet conditions in conventional SEM. Cem Concr Res. 2007;37:32–37.
[12] Smoczyński L, Ratnaweera H, Kosobucka M, et al. Image analysis of sludge aggregates. Sep Purif Technol. 2014;122:412–420.
[13] Lin JL, Huang C, Chin CJM, et al. Coagulation dynamics of fractal flocs induced by enmeshment and electrostatic patch mechanisms. Water Res. 2008;42:4457–4466.
[14] Jarvis P, Jefferson B, Parsons S. The duplicity of floc strength. Water Sci Technol. 2004;50:63–70.
[15] Jarvis P, Banks J, Molinder R, et al. Processes for enhanced NOM removal: beyond Fe and Al coagulation. Water Sci Technol Water Supply. 2008;8:709–716.
[16] Jarvis P, Jefferson B, Parsons SA. Breakage, regrowth, and fractal mature of natural organic matter flocs. Environ Sci Technol. 2005;39:2307–2314.
[17] Gonzalez-Torres A, Putnam J, Jefferson B, et al. Examination of the physical properties of *Microcystis aeruginosa* flocs produced on coagulation with metal salts. Water Res. 2014;60:197–209.
[18] Bridgeman J, Jefferson B, Parsons SA. Computational fluid dynamics modelling of flocculation in water treatment: a review. Eng Appl Comput Fluid Mech. 2009;3:220–241.
[19] Bridgeman J, Jefferson B, Parsons SA. The development and application of CFD models for water treatment flocculators. Adv Eng Softw. 2010;41:99–109.
[20] Bridgeman J, Jefferson B, Parsons S. Assessing floc strength using CFD to improve organics removal. Chem Eng Res Des. 2008;86:941–950.
[21] Samaras K, Zouboulis A, Karapantsios T, et al. A CFD-based simulation study of a large scale flocculation tank for potable water treatment. Chem Eng J. 2010;162:208–216.
[22] Prat OP, Ducoste JJ. Simulation of flocculation in stirred vessels lagrangian versus eulerian. Chem Eng Res Des. 2007;85:207–219.
[23] Prat OP, Ducoste JJ. Modeling spatial distribution of floc size in turbulent processes using the quadrature method of moment and computational fluid dynamics. Chem Eng. Sci. 2006;61:75–86.
[24] Vadasarukkai YS, Gagnon GA, Campbell DR, et al. Assessment of hydraulic flocculation processes using CFD. J Am Water Works Assoc. 2011;103:66–80.
[25] Argaman Y, Kaufman WJ. Turbulence and flocculation. J Sanit Eng Div. 1970;96:223–241.
[26] Bratby JR. Interpreting laboratory results for the design of rapid mixing and flocculation systems. AWWA Journal. 1981;73:318–325.
[27] Haarhoff J, Joubert H. Determination of aggregation and breakup constants during flocculation. Water Sci Technol. 1997;36:33–40.
[28] Tassinari B, Conaghan S, Freeland B, et al. Application of turbidity meters for the quantitative analysis of flocculation in a Jar test apparatus. J Environ Eng. 2015;141:1–8.
[29] Clark MM. Transport modeling for environmental engineers and scientists. 2nd ed. Hoboken: John Wiley & Sons; 2009.

[30] Fair GM, Gemmell RS. A mathematical model of coagulation. J Colloid Sci. 1964;19:360–372.
[31] Kramer TA, Clark MM. Incorporation of aggregate breakup in the simulation of orthokinetic coagulation. J Colloid Interface Sci. 1999;216:116–126.
[32] Kramer TA, Clark MM. Modeling orthokinetic coagulation in spatially varying laminar flow. J Colloid Interface Sci. 2000;227:251–261.
[33] Leentvaar J, Rebhun M. Strength of ferric hydroxide flocs. Water Res. 1983;17:895–902.
[34] Lu C, Spielman L. Kinetics of floc breakage and aggregation in agitated liquid suspensions. J Colloid Interface Sci. 1985;103:95–105.
[35] Parker DS, Kaufman WJ, Jenkins D. Floc breakup in turbulent flocculation processes. J Sanit Eng Div. 1972;98:79–99.
[36] Tambo N, Hozumi H. Physical characteristics of flocs – II. Strength of floc. Water Res. 1979;13:421–427.
[37] Wiesner MR. Kinetics of aggregate formation in rapid mix. Water Res. 1992;26:379–387.
[38] Jarvis P, Jefferson B, Gregory J, et al. A review of floc strength and breakage. Water Res. 2005;39:3121–3137.
[39] Henderson R, Parsons SA, Jefferson B. The impact of algal properties and pre-oxidation on solid-liquid separation of algae. Water Res. 2008;42:1827–1845.
[40] Henderson RK, Parsons SA, Jefferson B. The impact of differing cell and algogenic organic matter (AOM) characteristics on the coagulation and flotation of algae. Water Res. 2010;44:3617–3624.
[41] Teixeira MR, Rosa MJ. Comparing dissolved air flotation and conventional sedimentation to remove cyanobacterial cells of *Microcystis aeruginosa*. Part II. The effect of water background organics. Sep Purif Technol. 2007;53:126–134.
[42] Teixeira MR, Sousa V, Rosa MJ. Investigating dissolved air flotation performance with cyanobacterial cells and filaments. Water Res. 2010;44:3337–3344.
[43] Gorham PR, Mclachlan J, Hammer UT, et al. Isolation and culture of toxic strains of anabaena flos-aquae (lingb.). Verhandlungen des Internationalen Verein Limnologie. 1964;15:796–804.
[44] Henderson R, Chips M, Cornwell N, et al. Experiences of algae in UK waters: a treatment perspective. Water Environ J. 2008;22:184–192.
[45] Rice, EW, Baird, RB, Eaton, LS, et al., editors. Standard methods for the examination of water and wastewater. Washington, DC: American Public Health Association, American Water Works Association, Water Environment Federation; 2012.
[46] Jensen JN. A problem-solving approach to aquatic chemistry. Hoboken: John Wiley & Sons; 2003.
[47] Stumm W, Morgan JJ. Aquatic chemistry: chemical equilibria and rates in natural waters. New York: John Wiley & Sons; 1996.
[48] Chapra SC. Surface water-quality modeling. Long Grove: Waveland Press; 2008.
[49] Chapra SC, Canale RP. Numerical methods for engineers. 6th ed. New York: McGraw-Hill; 2010.
[50] Berthouex PM, Brown LC. Statistics for environmental engineers. 2nd ed. Boca Raton: Lewis Publishers; 2002.
[51] Hadjoudja S, Deluchat V, Baudu M. Cell surface characterisation of *Microcystis aeruginosa* and *Chlorella vulgaris*. J Colloid Interface Sci. 2010;342:293–299.